Catalysis Science & Technology

Accepted Manuscript

ROYAL SOCIETY OF CHEMISTRY

www.rsc.org/catalysis

Preparation and characterization of high oxygen storage capacity and thermally stable ceria-zirconia solid solution

Jie Li, Xiaofei Liu, Wangcheng Zhan, Yun Guo, Yanglong Guo, Guanzhong Lu*

* *Key Laboratory for Advanced Materials and Research Institute of Industrial Catalysis, East China University of Science and Technology, Shanghai, 200237, P. R. China.*

* Corresponding Author: Fax:+86-21-64252923. E-mail: gzhlu@ecust.edu.cn (G.Z. Lu).

Abstract: Ceria-zirconia solid solution is a very important material in the three-way catalyst for automotive emission control. High oxygen storage capacity (OSC) and thermally stabile $Ce_{0.5}Zr_{0.5}O_2$ was prepared by a modified complexing-coprecipitation (CC) method, and its surface area reached 44 m^2/g after calcination at 1100 °C for 6 h. Based on the characterizations of structural and physicochemical properties, it was found that $Ce_{0.5}Zr_{0.5}O_2$ prepared by the CC method existed as the *t*''-phase with rich oxygen defects and surface Ce^{3+}, and has bigger BET surface area, uniform particle and pore sizes, excellent bulk oxygen migration and redox abilities than the samples prepared by other methods. After being calcined at 1100 °C for 6 h, its surface area, OSC (and OSCC, oxygen storage capacity complete) and catalytic activity for the oxidation of CO was still the best among three $Ce_{0.5}Zr_{0.5}O_2$ solid solutions prepared by three methods whether it was used as the catalyst or support for Pd catalyst, reflecting its good thermostability, though its particle and pore size was some increased. This complexing-coprecipitation method can be used to prepare the high surface area and thermally stabile other inorganic materials.

Keywords: $Ce_{0.5}Zr_{0.5}O_2$ solid solution; Oxygen Storage Capacity; Complexing-coprecipitation method; High thermal stability.

1. Introduction

Ceria-zirconia solid solution (CZSS) has attracted more interests recently due to its extensive applications in the catalytic processes [1-13]. As the oxygen storage materials CZSS has been used in three-way catalysts (TWCs) for the catalytic purification of CO, NOx and hydrocarbons (HC) from automobile exhausts, and the presence of CZSS can enlarge the stoichiometric window of air-to-fuel in TWCs by the help of its outstanding redox ability, in other word, its excellent oxygen storage/release capacity [14-17]. In the CZSS, the oxygen storage/release is circularly completed through the Ce^{4+}/Ce^{3+} couple ($CeO_2 \leftrightarrow CeO_{2-x} + (x/2)\ O_2$; x = 0~0.5) [18]. However, pure ceria is not very usable because of its relatively low OSC (oxygen storage capacity) and poor thermal stability [19,20], and the incorporation of ZrO_2 (Zr^{4+}) into the ceria lattice significantly effects the ceria performances by enhancing the thermal resistance, increasing the OSC [1,21]. Many research works were focused on the composition of CZSS and the preparation methods, in order to gain a high oxygen storage capacity and thermal stabile CZSS [22]. Our research results based on DFT+U calculations for the formation of O vacancies in a series of $Ce_{1-x}Zr_xO_2$ materials show that the formation energy of the O vacancy is dependent on the bond energy (E_{bond}) and relaxation energy (E_{relax}). And $Ce_{0.5}Zr_{0.5}O_2$ possesses the lowest formation energy of the O vacancy.[23]

With the increasingly strict regulations requiring lower emission standards of automotive vehicles, the catalytic performances of three-way catalysts should be further improved. Therefore, the oxygen storage/release ability and thermal stability of CZSS materials must be improved. Now, many research groups have already prepared by various ceria-based materials with different methods, and the CZSS with various degrees of homogeneity, and crystal and textual properties were reported [24]. The reported preparation methods include coprecipitation [25,26], hydrothermal process [27,48], sol-gel means [28-31] and other auxiliary methods, such as supercritical, surfactant and shape-controlled techniques [32-34]. In addition, other rare earth elements are also doped into CZSS for enhancing its structural and physiochemical properties [35-40]. The CZSS prepared by Raju *et al.* [41] has the surface area of ~12 m^2/g after calcination

at 1000 °C by continuous hydrothermal treatment, and the highest OSC of the $Ce_{0.5}Zr_{0.5}O_2$ solid solution reached 0.58 mmol [O]/g after calcination at 700 °C. Wang *et al*. [36] studied the effect of La doping into the CZSS, and found that the presence of doped La can enhance its BET surface area and OSC value. An analogous conclusion was reported by Yan *et al*.[42] These results show that, the aliovalent substitution of trivalent ions is deemed to stabilize the *t"* structure, which is believed to improve the thermal stability and OSC. Furthermore, Letichevsky *et al*. studied the effect of synthesis conditions on the properties of CZSS, and found that cerium precursor has the most significant influence on the preparation procedure, and the positive function of pH controlling cannot be neglected [25]. Nevertheless, the oxygen storage capacity and thermal stability of the CZSS materials should be further improved, and the *k*-$Ce_2Zr_2O_8$ CZSS has not been synthesized successfully, which has the outstanding OSC comparing with ordinary or commercial CZSS materials by a verification of our DFT calculation.[43]

Herein, we selected the $Ce_{0.5}Zr_{0.5}O_2$ solid solution as the model compound, because of its higher oxygen mobility and thermal stability[41,44-46], and try to design a new synthesis method (the complexing-coprecipitation, CC method) combined with controlling the pH value of the mixed precursor solution to realize the preparation of high oxygen storage capacity and thermal stable CZSS. Through their physicochemical and redox properties, and catalytic activity for the CO oxidation were investigated and compared with the ordinary CZSS prepared by Co-precipitation (CP) method, the relationship between the preparation method – structure (including thermal stability) – physicochemical properties (including oxygen storage capacity and catalytic performance) has been discussed in detail.

2. Experimental section

2.1. Preparation of sample

$Ce_{0.5}Zr_{0.5}O_2$ solid solution was prepared by three methods. (1) **Co-precipitation (CP) method**. $Ce(NO_3)_3 \cdot 6H_2O$ and $Zr(NO_3)_4 \cdot 5H_2O$ (Ce/Zr = 1, mol) were dissolved in de-ionized water under

stirring until the settled solution (1) formed. Then the ammonium hydroxide (25 Vol%.) was added dropwise into the above solution, and the pH value was controlled to be 10 finally. After PEG200 surfactant (PEG200/Ce = 0.1, mol) was added, the synthesis solution was continually stirred for 3 h. After being aged at room temperature for 24 h, the formed precipitate was filtered and washed with deionized water until the pH value of eluate was unchanged. Then this yellow precipitate was dried at 110 °C for 2 h.

(2) Complexing-coprecipitation (CC) method. Before the ammonium hydroxide was added in the solution (1), citric acid monohydrate (citric acid/(Ce+Zr) = 1.2, mol) dissolved into the synthesis solution, and subsequently ammonium hydroxide (25 Vol.%) was added to adjust pH = ~3. Then PEG200 surfactant (PEG200/Ce = 0.1, mol) was added, this solution was continually stirred for 3 h, and the solution (2) including white precipitate was formed. The white precipitate was filtered, washed with deionized water until the pH value of eluate was unchanged. Then this white precipitate was dried at 110 °C for 2 h.

(3) **Complexing-coprecipitation-solution (CCS) method**. With an increase in the pH value of the solution (2) by adding ammonia, the white precipitate was slowly dissolved in the solution. After the pH value reached ~10 and PEG200 surfactant (PEG200/Ce = 0.1, mol) was added under stirring, it was taken into the drying oven (80 °C) overnight.

Finally, three samples were calcined in static air at 500 °C for 4 h. The obtained fresh samples were denoted as CZ-1, CZ-2, CZ-3, respectively. The fresh samples were further calcined at 1100 °C for 6 h in dry air to obtain aged samples (CZ-1a, CZ-2a, and CZ-3a).

2.2. Preparation of Pd/CZ catalysts

Pd/CZ catalysts were prepared by the incipient impregnation method with aqueous solutions of $Pd(NO_3)_2$ as the metal precursors (Pd loading was 1 wt.%). The catalysts were dried at 50 °C overnight and calcined at 500 °C for 2 h. These fresh catalysts were named as Pd/CZ-1, Pd/CZ-2 and Pd/CZ-3, respectively. After the catalysts were aged at 1100 °C for 6 h in dry air, they were denoted as Pd/CZ-1a, Pd/CZ-2a and Pd/CZ-3a, respectively.

2.3. Characterization of sample

The powder X-ray diffraction (XRD) patterns were collected on a Bruker D8 Focus diffractometer with Cu Kα radiation (λ=1.54056 Å, operated at 40 kV and 40mA). The average crystalline size and the lattice parameter of sample were determined by the Scherrer formula based on the diffraction peak broadening of (111) plane.

Laser Raman spectra (LRS) of samples were collected on a LabRAM-HR Raman spectrograph equipped with a CCD detector at ambient condition. An Ar ion laser beam (λ= 514 nm) was used for an excitation and the spectral resolution was 4 cm^{-1}.

Nitrogen adsorption-desorption isotherms were measured at −196 °C on a Quantachrome NovaWin2 sorption analyzer. Before the measurement, all the samples were outgassed to remove moisture and impurities at 200 °C under vacuum for 10 h. Brumauer-Emmett-Teller (BET) method was used to calculate the specific surface areas of samples. Pore size distribution curves were derived from desorption branches of the isotherms and calculated by the Barrett-Joyner-Halanda (BJH) method.

Scanning electron microscopy (SEM) images were taken on a JEOL JSM-6360LV scanning electron microscope operated at 20 kV. The sample was flattened by sprinkling the powder oxides onto double-sided sellotape and mounted on a microscope stub without any further treatment. Transmission electron microscopy (TEM) images were recorded on a JEOL 1400F electron microscope operated at 200 kV, and the sample to be measured was first dispersed in ethanol and then collected on copper grids covered with carbon film.

The X-ray photoelectron spectroscopy (XPS) spectra were obtained at 25 °C on a PHI-Quantera SXM spectrometer with Al Kα (1486.6 eV) radiation as the excitation source at ultra-high vacuum (6.7×10^{-8} Pa). All binding energies (BE) were determined with respect to the C1s line (284.8 eV) originating from adventitious carbon. The powder samples were pressed into self-supporting disks loaded in the sub-chamber, and evacuated for 4 h. The deconvolution method of XPS spectra was fitted by Gaussian function with the software named XPSPEAK 4.1.

H_2 temperature-programmed reduction (TPR) was carried out on a TPDRO 1100 (CE Instruments). After 50 mg catalyst was swept in the flow of 5 vol.% H_2/N_2 (40 ml/min) at room temperature for several minutes, H_2-TPR was run at a heating rate of 10 °C/min from room temperature to 800 °C or 900 °C. The amount of H_2 uptake in the reduction process was measured by the thermal conductivity detector (TCD).

Oxygen storage/realease capacity of catalyst was measured by CO pulse injection on a Micromecitics AutoChem II 2920 chemisorption analyzer with He as carrier gas. Prior to the measurement, 30 mg sample was firstly treated in the flow of 3%O_2/He (50 ml/min) from room temperature to 550 °C at a rate of 10 °C/min and maintained at 550 °C for 1 h. Subsequently, the sample was cooled down to 400 °C in He flow and purged with He for 30 min. Then quantitative 5% CO/He was injected into the sample cell every 2 min in the carrier gas of He (50 ml/min) until CO was no longer consumed, to obtain the pulse curves. The total amount of CO uptake (O_2 release) on a series of CO pulses was defined as the oxygen storage capacity complete (OSCC). And the amount of CO uptake upon the first CO pulse was defined as OSC (the oxygen storage capacity) [47], which is attributed to the most reactive and the most available oxygen. OSC and OSCC were both expressed as μmol of [O] per gram of catalyst (μmol[O]/g).

2.4. Catalytic activity testing

The catalytic activity of sample for CO oxidation was tested in a home-made fixed-bed micro-reactor (a quartz tube with an inner diameter of 6 mm) at atmospheric pressure. 100 mg catalyst was used and the reactant gas was consisted of 1000 ppm CO + 20% O_2/Ar balanced (50 ml/min) or 1000 ppm CO + (20% O_2 + 5% H_2O)/Ar balanced (50 ml/min). The gaseous hourly space velocity (GHSV) was 30000 h^{-1}. The composition of the influent and effluent gas was detected by online GC2060 gas chromatograph equipped with a flame ionization detector (FID), in which a methanizer was used for hydrogenating CO_2 and CO to methane. The CO conversion was calculated as follows: Conversion of CO = $(CO_{in} - CO_{out})/CO_{in} \times 100\%$, CO_{in} and CO_{out} are the CO concentration in the inlet and outlet, respectively.

3. Results and discussion

3.1. Structure and textual properties

The XRD patterns of the fresh and aged samples are shown in Fig. 1. The average crystallite size and the lattice parameter are also exhibited in Table 1. The results show that the XRD diffraction peaks of all the samples are consistent with the characteristic peaks of either cubic CeO_2 or an intermediate phase *t"*-phase, which cannot be assigned accurately due to the broader peaks, but these diffraction peaks are the same as those of cubic solid solution of $Ce_{0.5}Zr_{0.5}O_2$ [51].

Generally speaking, a quite whole phase diagram of ceria-zirconia mixed oxides contains three stable phases (monoclinic (m), tetragonal (t) and cubic (c)) and two metastable tetragonal phases (*t'* and *t"*) [41,42,49,50]. Among them, *t*-phase is formed through a diffused phase decomposition, *t'*-phase is taken from a diffusionless transition, and the pseudo-cubic *t"*-phase is an intermediate phase between *t'* and *c*, and its structure is very close to that of cubic *c*-phase. Both the *t'*-phase and the *t"*-phase have the same space group of $P4_2/nmc$. With regard to three fresh samples, the diffraction peaks (Fig. 1A) are corresponding to the characteristic peaks of cubic *c*- or *t"*-phase with a space group of $P4_2/nmc$. As the nano-crystalline size effect, the widths of diffraction peaks are very broad, ~2.0°, making it difficult to distinguish the presence of the matastable tetragonal phases where. Usually, the expected splitting constants are less than 1.0° [51].

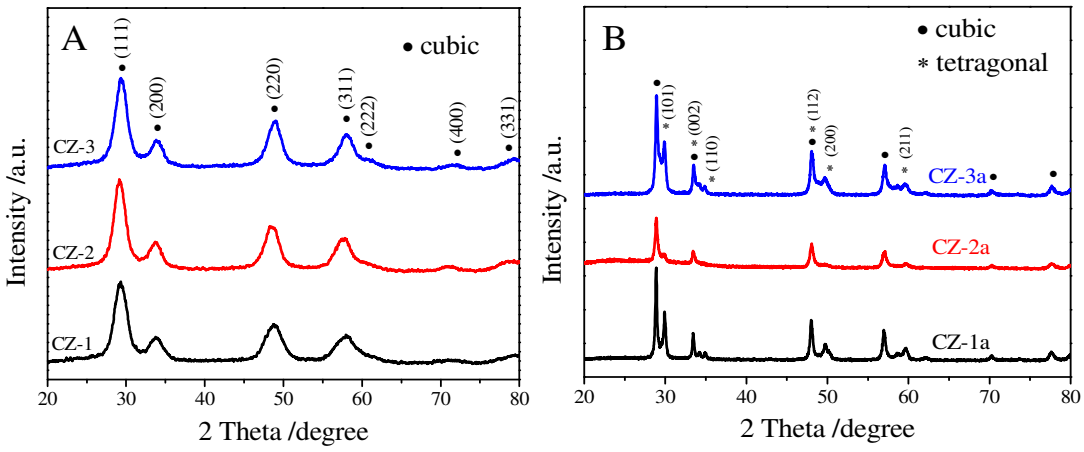

Fig. 1. XRD patterns of (A) fresh and (B) aged $Ce_{0.5}Zr_{0.5}O_2$ solid solutions prepared by different methods.

However, compared with pure CeO_2, the diffraction peaks of three fresh samples shifted to

higher 2θ, indicating that the incorporation of Zr^{4+} into the CeO_2 lattice [52,53]. The lattice constants of CZ-1, CZ-2 and CZ-3 were calculated and 5.241, 5.346 and 5.304 nm respectively, which can be ranked in the order of CZ-1 < CZ-3 < CZ-2, while their crystallite sizes (Table 1) were varied as an entirely opposite sequence of CZ-1 > CZ-3 > CZ-2. These results make us speculate that CZ-2 ought to be the most homogeneous solid solution consisted of highly dispersed nanoparticles.

Table 1. Textural properties of fresh (calcined at 500 °C) and aged (at 1100 °C) $Ce_{0.5}Zr_{0.5}O_2$ solid solutions.

Sample	Surface area (m^2/g)	Pore volume (cm^3/g)	Average pore diameter (nm)	Crystal size (nm)	Lattice parameter (Å)
CZ-1	61.4	0.216	6.02	5.90	a=5.241
CZ-2	136	0.790	5.07	4.80	a=5.346
CZ-3	126	0.729	7.32	5.00	a=5.304
CZ-1a	13.5	0.112	30.5	37.3	a=3.788, c=5.358
CZ-2a	43.9	0.408	18.9	21.6	a=3.786, c=5.359
CZ-3a	26.8	0.309	19.4	26.3	a=3.599, c=5.345

For the aged samples, after thermal treatment, all diffraction peaks became narrower and sharper (Fig. 1b), indicating that the crystallite size of the aged samples increased (Table 1). As shown in Fig. 1B, the diffraction peaks of Zr-rich phase (ZrO_2, *t*) could be detected obviously in the XRD patterns of both CZ-1a and CZ-3a, but these diffraction peaks of tetragonal phase are very weak for CZ-2a, while their lattice constant of the cubic phase increased and there have been the lattice constant of the tetragonal phase. The average crystallite sizes of these samples determined by Scherrer equation were increased in the order of CZ-2 (21.6 nm) < CZ-3 (26.3 nm) < CZ-1 (37.3 nm). It is easy to find that the smaller particle size, especially the smallest particle size of CZ-2 among three samples, can be obtained by the complexing-coprecipitation method, that is to say, the complexing-coprecipitation method is the effective method for preparing high stable $Ce_{0.5}Zr_{0.5}O_2$ solid solution, which can inhibit thermal sinter of oxide particles and retard the separation of Ce-rich and Zr-rich phases at high temperatures.

As is well-known, Raman spectroscopy is a sensitive tool to detect the crystal defect, and the

Raman spectra of $Ce_{0.5}Zr_{0.5}O_2$ solid solutions prepared with different methods are shown in Fig. 2. For the fresh samples, four peaks located at ~138, 312, 476, 630 cm^{-1} of CZ-2 are attributed to the *t''*-phase. And CZ-1 and CZ-3 have a strong broad band at 467 cm^{-1} with three bands at 138, 312 and 640 cm^{-1}, which are originated from the six Raman active modes (A_{1g} + $2B_{1g}$ + $3E_g$) of the *t*-phase (or *t*-ZrO_2, space group $P4_2/nmc$), and the strongest peak at 467 cm^{-1} is also related to the Raman active mode (F_{2g}) of the *c*-phase, resulting from the oxygen vacancies created upon Ce^{4+} substitution by Zr^{4+} ion insertion to form the CeO_2-ZrO_2 solid solution accompanied by the lattice shrinkage [51]. For the aged samples, five bands at 138, 256, 312, 476 and 630 cm^{-1} in the spectra of CZ-1a and CZ-3a can be assigned to the tetragonal ZrO_2 (*t*-ZrO_2), and the strongest peak at 476 cm^{-1} with three small peaks at 138, 312 and 630 cm^{-1} from CZ-2a can be also attributed to the Raman active mode (F_{2g}) of the *t''*-phase or/and *c*-phase [42].

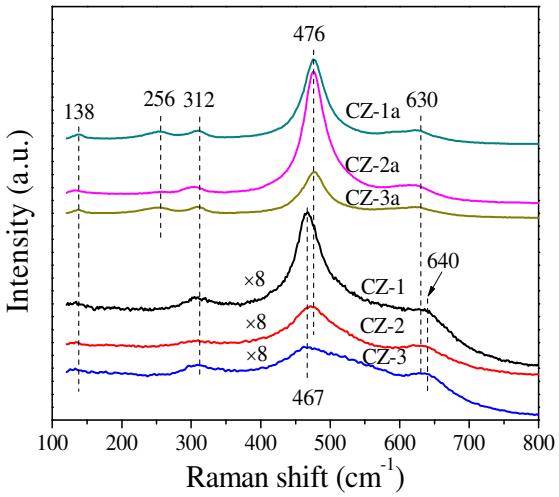

Fig. 2. Raman spectra of fresh and aged $Ce_{0.5}Zr_{0.5}O_2$ samples.

Based on the results of XRD in Fig.1 and Raman spectra in Fig. 2, we can see that the CZ-1 and CZ-3 samples were composed of a mixed phases of *t*- and *c*-phase, and the CZ-2 sample was mainly attributed to the *t''*-phase, and the *t''*-phase has a defective structure containing rich oxygen vacancies [54]. Therefore, we expect that CZ-2 possesses more excellent redox performance or OSC/OSCC property than other CZ samples. After being calcined, CZ-2a, unlike CZ-1a and CZ-3a, behaved better in inhibiting the phase separation at high temperature, and existed at

t''-phase and *c*-phase, which is consistent with the results of XRD measurement.

The N_2 adsorption/desorption isotherms of fresh samples are shown in Fig. 3. As seen in Fig. 3, the N_2 absorption/desorption isotherms of CZ-2 and CZ-3 are attributed to IV-type isotherm with an H1-type hysteresis loop [37], indicating the formation of large interparticle mesopores both at the external surface and in the inner region of the agglomerates, and CZ-1 displays the IV-type isotherm with an H2-type hysteresis loop, which arises from the presence of mesopores texture and ink-bottle shaped pores [54]. From these two types of hysteresis loops, it can be found that samples prepared by the complexing-coprecipitation (CC) method can avoid the collapse of the pore walls and form more porous structures.

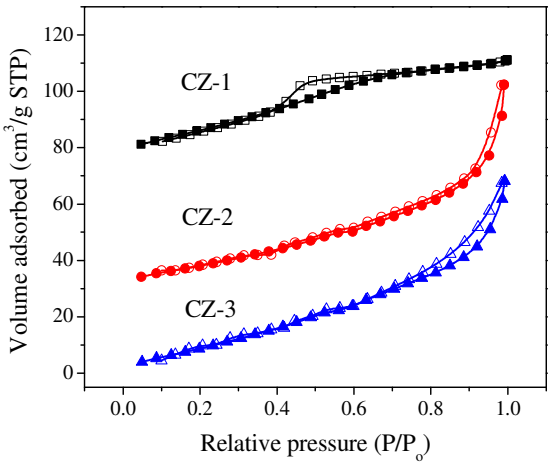

Fig. 3. Nitrogen adsorption/desorption isotherms of fresh $Ce_{0.5}Zr_{0.5}O_2$ samples prepared with different methods.

Table 1 lists the BET surface area, average pore diameter calculated by the Barrett-Joyner-Halenda (BJH) method, and total pore volume of $Ce_{0.5}Zr_{0.5}O_2$ samples. The results show that CZ-2 has the biggest surface area and pore volume compared with that of other samples. The pore volume of CZ-2 (including CZ-2a) is even three times as large as that of CZ-1 (or CZ-1a), indicating that the addition of citric acid in the process of complexing-coprecipitation has fabricated various kinds of pores due to the extravasation of carbon species gas during calcination.

As shown in Table 1, after being aged, the specific surface areas of $Ce_{0.5}Zr_{0.5}O_2$ were reduced obviously, because of severe aggregation of nano-particles, and their accumulative pore volume

were also remarkably decreased. Compared with other samples, however, CZ-2a maintains higher surface area and larger pore volume after calcination, that is to say, its pore structure has not collapsed entirely, indicating the good thermal stability of CZ-2. The pore diameter distribution curves of fresh and aged samples are shown in Fig. 4. For fresh samples, CZ-2 behaves more homogeneous texture with the pore diameter of ~4 nm (most probable pore diameter), and the curve of CZ-1 is similar to one of CZ-3. After being aged, CZ-2a exhibits the smallest pore diameter of ~23 nm (10–50 nm), second is CZ-3a with pore diameter of ~50 nm (10~80 nm), and CZ-1a has largest pore of ~ 60 nm (30–90 nm).

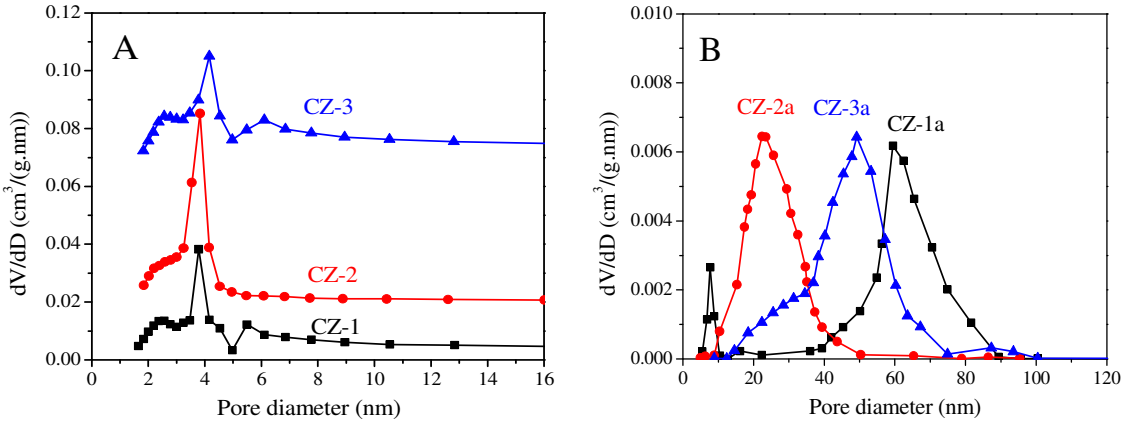

Fig. 4. Pore diameter distribution curves of (A) fresh and (B) aged $Ce_{0.5}Zr_{0.5}O_2$ samples prepared with different methods.

3.2. XPS measurement

Three $Ce_{0.5}Zr_{0.5}O_2$ samples were tested by XPS, and their XPS spectra of Ce 3d are shown in Fig. 5, which could be fitted with eight peaks corresponding to four pairs of spin-orbit doublets [55,56]. u and v refer to the $3d_{3/2}$ and $3d_{5/2}$ spin-orbit components respectively, and its spin-orbit splitting is 18.4 eV [57]. The peaks of u (901.2–901.8 eV), u'' (907.7–908.3 eV) and u''' (916.7–917.3 eV) arose from Ce^{4+} $3d_{3/2}$, while the peaks labeled as v (882.8–883.2 eV), v'' (889.1–889.7 eV) and v''' (898.5–899.0 eV) arose from Ce^{4+} $3d_{5/2}$. The peaks of u' (903.6-904.3 eV) and v' (885.2-885.8 eV) should be ascribed to the Ce^{3+} species. Therefore, the proportion of Ce^{3+} cation in the total cerium was calculated based on the ratio of the sum of areas of the Ce^{3+}

species (u', v') to the sum of areas of the total cerium species (u, u', u'', u'''; v, v', v'', v''') and listed in Table 2.

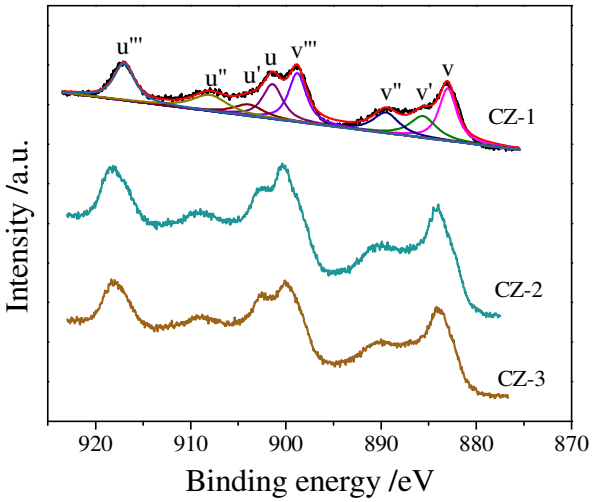

Fig. 5. Ce 3d XPS spectra of the $Ce_{0.5}Zr_{0.5}O_2$ samples prepared by different methods.

Table 2. Surface elemental compositions of CZ samples derived from XPS data.

Sample	Surface composition (atom %)			Ce/Zr (mol)	Ce^{3+}/Ce (%)
	Ce 3d	Zr 3d	O 1s		
CZ-1	9.3	10.6	54.6	0.88	20.0
CZ-2	11.2	8.8	55.9	1.27	21.4
CZ-3	9.8	10.5	54.9	0.93	19.3
CZ-1a	9.8	11.2	65.6	0.87	19.3
CZ-2a	10.8	9.9	64.8	1.09	20.9
CZ-3a	10.0	10.1	63.9	0.99	18.7

The surface elemental components of the catalysts were calculated on the normalized peak areas of the Ce 3d, Zr 3d, O 1s core level spectra are listed in Table 2. As shown in Table 2, the surface content of Ce element was descended in the order of CZ-2 > CZ-3 > CZ-1, and only the surface Ce/Zr atomic ratio of CZ-2 sample is higher than the theoretical atomic ratio of 1.0, which means that Ce is enriched on the surface layer. While the related surface content of Ce^{3+} is the highest comparing with CZ-1 and CZ-3, and CZ-2 > CZ-1 > CZ-3, which represents that CZ-2 has the most oxygen vacancies on the surface and highest oxygen mobility, because the presence of Ce^{3+} resulted from the formation of oxygen vacancy.[58] As for the aged samples, the surface content

of Ce^{3+} in CZ-2 was the highest among three samples, demonstrating the highly thermal stability of CZ-2 solid solution.

3.3. Morphologies of samples

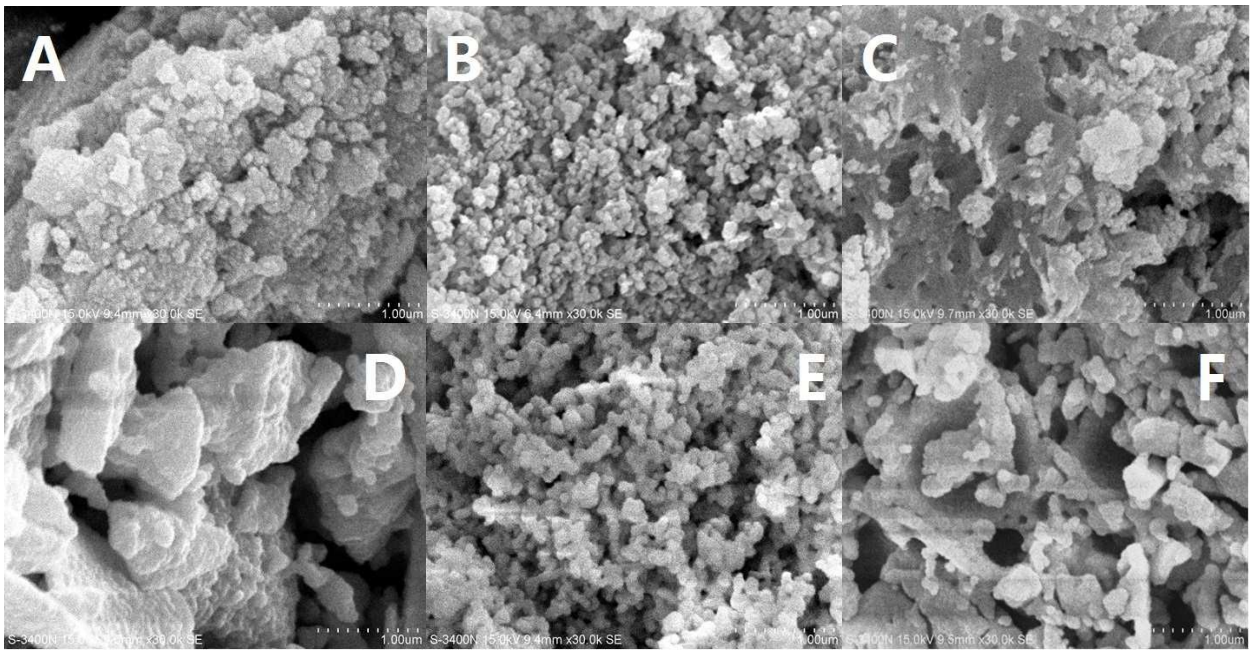

Fig. 6. SEM images of (A) CZ-1, (B) CZ-2, (C) CZ-3, (D) CZ-1a, (E) CZ-2a and (F) CZ-3a.

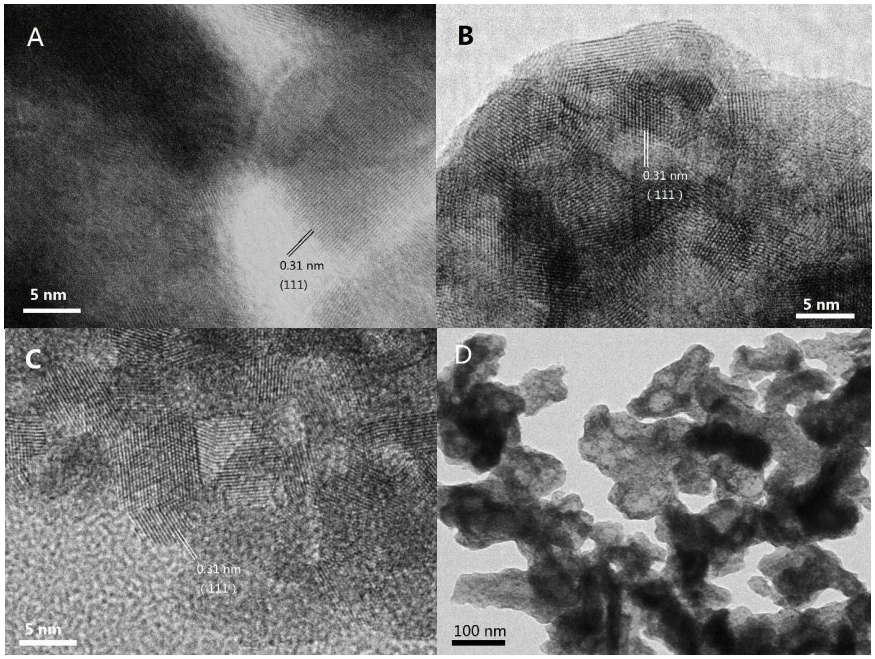

Fig. 7. HR-TEM images of aged samples (A) CZ-1a, (B) CZ-2a, (C) CZ-3a, and (D) CZ-2a.

The morphologies of samples were investigated by SEM, and the results are shown in Fig. 6.

For the fresh samples, they exhibit different surface morphologies, due to different preparation methods. CZ-1 prepared by the CP method exhibits the close aggregation of random particles, and after calcination at 1100 °C for 6 h, its particles increased remarkably because of sintering. And the surface of CZ-3 prepared by the CCS method was consisted of rambling particles and pore channels, after aged at 1100 °C for 6 h its particles and pore channels were some enlarged but became uniform. Comparing with CZ-1 and CZ-3, the surface of CZ-2 was consisted of homogeneous particles with a narrow size range by incompact aggregation. After calcination at 1100 °C for 6 h, its morphology was hardly changed except the increasing of particles accompanied with the expansion of pore sizes, which shows CZ-2 possesses much better sintering resistance (Fig. 7D), in which massive particles and compact agglomeration can be observed apparently. As shown in the HR-TEM images (Fig. 7), the exposed crystal faces were mainly the (111) facet and the interplanar spacing is 0.31 nm for three aged samples, although their preparation method were different.

3.4. Reducibility and OSC properties

3.4.1. H_2-TPR

The TPR profiles of fresh and aged $Ce_{0.5}Zr_{0.5}O_2$ solid solutions are shown in Fig. 8, and their total amounts of H_2 consumption were calibrated with standard CuO sample and listed in Table 3. For three fresh samples, there are two broad reduction peaks, the low temperature (α) peaks at 385-425 °C and the high temperature (β) peaks at 485-525 °C, which can be ascribed to the reduction of Ce^{4+} (surface Ce^{4+} and bulk Ce^{4+}) [51]. The reduction temperature of surface Ce^{4+} is generally at < 400 °C, but it cannot be distinguished clearly from the reduction of bulk Ce^{4+} [59]. Therefore, the α peak should be ascribed to the reduction of surface Ce^{4+} (or oxygen) and the β peak is to the reduction of bulk Ce^{4+} (or lattice oxygen). Note that the different preparation method affected the areas and positions of reduction peaks of samples, in which CZ-2 has the largest peak area and CZ-1 exhibits the lowest top temperature of α peak. On the basis of TPR profiles, the

reducibility of CZ solid solution ranked in a sequence of CZ-2 > CZ-3 > CZ-1, which shows that fresh CZ-2 has the fast bulk oxygen mobility and best reducibility.

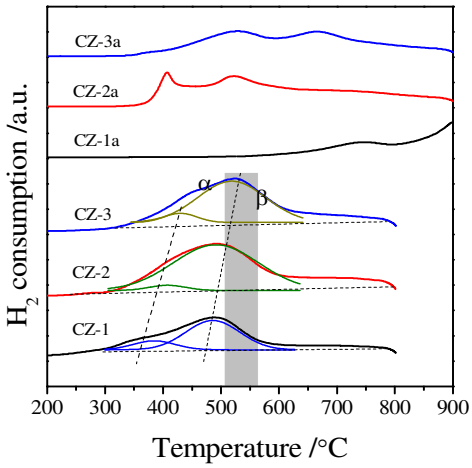

Fig. 8. TPR profiles of fresh and aged $Ce_{0.5}Zr_{0.5}O_2$ solid solutions prepared by different methods.

For the aged samples, there are different TPR profiles with two reduction peaks. In the TPR profile of CZ-1a, two peaks appeared at 750 ℃ and 900 ℃ respectively and should be ascribed to the reduction of bulk oxygen of ceria. Thus it follows that the separation of Ce-rich and Zr-rich phase has produced after calcination at 1100 °C. In the TPR curves of CZ-2a and CZ-3a, there are two reduction peaks, but their top temperatures are completely different. Two top temperatures of CZ-2a are almost the same as these of CZ-2, but the reduction peaks of CZ-3a have shifted to higher temperature about 120-140 °C. These results show that, the CZ-2 sample prepared by the complexing-coprecipitation (CC) method is a high thermal stable, which should be attributed to its smaller crystallites (Table 1) among three aged samples at 1100 °C, because of easier reduction of smaller crystallites for $Ce_{0.5}Zr_{0.5}O_2$ solid solution.[36,47]

3.4.2. OSC and OSCC

In order to study the total oxygen amount available and bulk oxygen mobility of the CZ sample, the CO/He pulse was used and their pulse profiles of fresh samples are depicted in Fig. 9, and Fig. 9D show that the CO consumption in each CO pulse as a function of number of pulse. It was defined as the total amount of CO uptake (O_2 release) to be the oxygen storage capacity complete

(OSCC), and the amount of CO uptake upon the first CO pulse to be the oxygen storage capacity (OSC). Thus, the OSC and OSCC values of samples were measured at 400 °C and listed in Table 3. For the fresh samples, their OSC and OSCC are varied in the order of CZ-2 > CZ-1 > CZ-3, and after being aged at 1100 °C, the OSC and OSCC are ranked as follows: CZ-2a > CZ-3a > CZ-1a. Therefore, the sample prepared by the complexing-coprecipitation (CC) method possesses the best oxygen storage capacity among three samples.

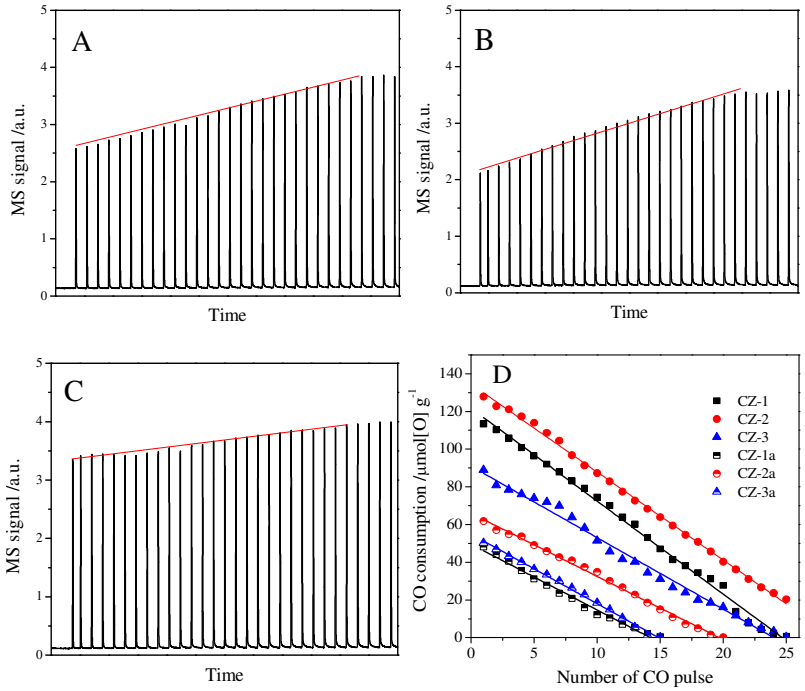

Fig. 9. CO pulse testing over (A) CZ-1, (B) CZ-2, (C) CZ-3, and (D) the CO consumption in each pulse as a function of number of CO pulse at 400 °C.

Table 3. The OSC and OSCC values of fresh and aged $Ce_{0.5}Zr_{0.5}O_2$ samples at 400 °C.

Sample	OSC[a] (μmol[O]/g)	OSCC (μmol[O]/g)	
		Pulse experiment[b]	H_2-TPR[c]
CZ-1	113	874	820
CZ-2	128	1205	1145
CZ-3	89	954	1034
CZ-1a	48	320	300
CZ-2a	62	615	527
CZ-3a	50	350	450

[a] The amount of CO uptake upon the first CO pulse after fully oxidized with O_2 at 400 °C.
[b] The amount of CO uptake upon all CO pulses after fully oxidized with O_2 at 400 °C.
[c] The amount of H_2 consumption in the TPR process, which were calibrated with the CuO reduction as a standard.

3.5. CO oxidation

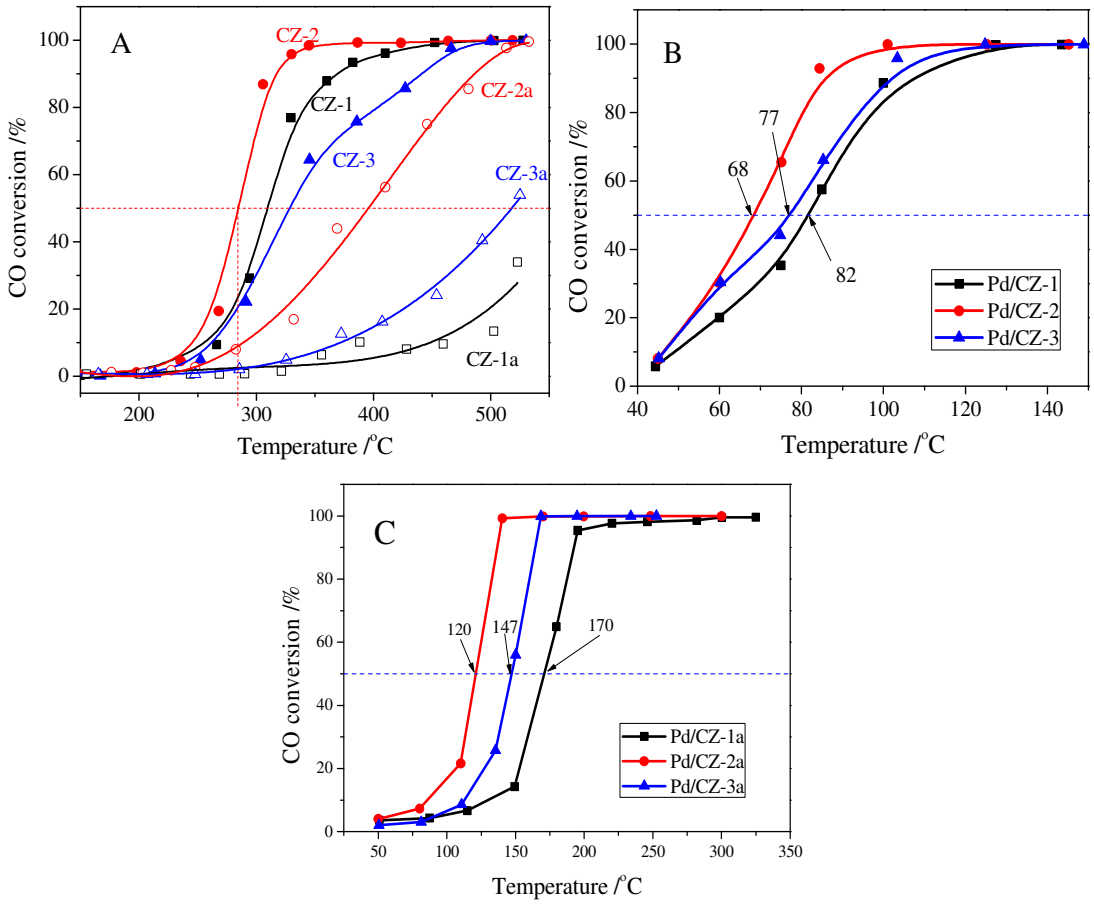

Fig. 10. Conversion of CO over (A) fresh and aged CZ, (B) fresh and (C) aged 1wt.%Pd/CZ. (1000 ppm CO + 20% O_2/Ar, GHSV of 30000 h^{-1})

The CO oxidation was used as a model reaction to evaluate the effect of preparation method on the catalytic property and thermal stability of the $Ce_{0.5}Zr_{0.5}O_2$ solid solution. As shown in Fig. 10A, the catalytic activities of fresh CZ samples are decreased in order of CZ-2 (T_{50} = 285 °C) > CZ-1 (310 °C) > CZ-3 (328 °C), T_{50} is the reaction temperature of 50% CO conversion, which is the same as their rank for OSC and OSCC. For the aged samples, a variation of their catalytic activities is also the same as their OSC and OSCC: CZ-2a > CZ-3a > CZ-1a. These results show that the catalytic activity of $Ce_{0.5}Zr_{0.5}O_2$ solid solution for CO oxidation is tightly ascribed to its surface oxygen reducibility and bulk oxygen mobility, and the CZ-2 prepared by complexing-coprecipitation (CC) method exhibits the best reducibility and oxygen mobility.

The catalytic activities of the fresh and aged 1%wt.Pd/CZ catalysts for CO oxidation are shown in Fig. 10B, C. The results show that T_{50} of these fresh samples was ranked in the following order of Pd/CZ-2 (T_{50} = 68 °C) < Pd/CZ-3 (77 °C) < Pd/CZ-1 (82 °C). After the 1%Pd/CZ was calcined at 1100 °C for 6 h, T_{50} of Pd/CZ-2a was raised to 120 °C and the activity of Pd/CZ-1a was declined obviously, its T_{50} reached to 170 °C. These results show that as a support of Pd catalyst the CZ-2 solid solution is better than other two samples, which should be attributable to its high thermostability, including large surface area, high OSC or reducibility, and small particle sizes. The effect of the CZSS nature on the physicochemical properties and the interaction between Pd species and CeO_2-ZrO_2 support will be deeply and systematically investigated.

As shown in Fig. 11, when the feed gas containing 5%H_2O, the catalytic activities of fresh CZ samples were some dropped, and their T_{50} was changed in the order of CZ-1 (330 °C) ≈ CZ-2 (340 °C) > CZ-3 (400 °C). After the CZ samples were aged at 1100 °C for 6 h, their catalytic activities were decreased remarkably, for instance, T_{50} of CZ-2a and CZ-3a reached to 515 °C, and the catalytic activity of CZ-1a was very low: only 20% CO conversion at 650 °C. For the Pd/CZ samples, it is interesting that T_{50} of Pd/CZ-2 and Pd/CZ-1 was only 50 °C in the presence of 5%H_2O and obviously lower than their T_{50} (68 °C over Pd/CZ-2, and 82 °C over Pd/CZ-1) without water, and T_{50} of Pd/CZ-3 was 70 °C in the presence of 5%H_2O and lower than that (77 °C) without water, which show that the presence of H_2O could increase the catalytic activity of Pd/CZ catalysts for the CO oxidation. After being aged at 1100 °C for 6 h, T_{50} of Pd/CZ-2a (or Pd/CZ-3a) raised from 50 °C (or 70 °C) to 70 °C (or 110 °C), and the catalytic activity of Pd/CZ-1a was insanely dropped and its T_{50} reached 255 °C. This is because that in the process of CO reacting with lattice O, the H_2O molecule also reacts with CO forming absorbed intermediate, COOH(ad), which can be decomposed to CO_2 and H. And then, the H from H_2O and COOH react with the absorbed O to form H_2O and CO_2.[60]

Now, we conclude that when these catalysts were used in the feed gas with 5%H_2O, the performance of CZ-2 almost be same as that of CZ-1 as the catalyst or support for Pd catalyst for

the CO oxidation. And for the CZ samples aged 1100 °C for 6 h, and CZ-2a prepared by the complexing-coprecipitation method exhibits much higher thermostability than that of CZ-1a prepared by the co-precipitation method, especially when CZ was used as the support for Pd catalyst. Therefore, we can supply the high-performance and thermal stabile ceria-zirconia solid solutions for the three-way catalysts for automobile emission control.

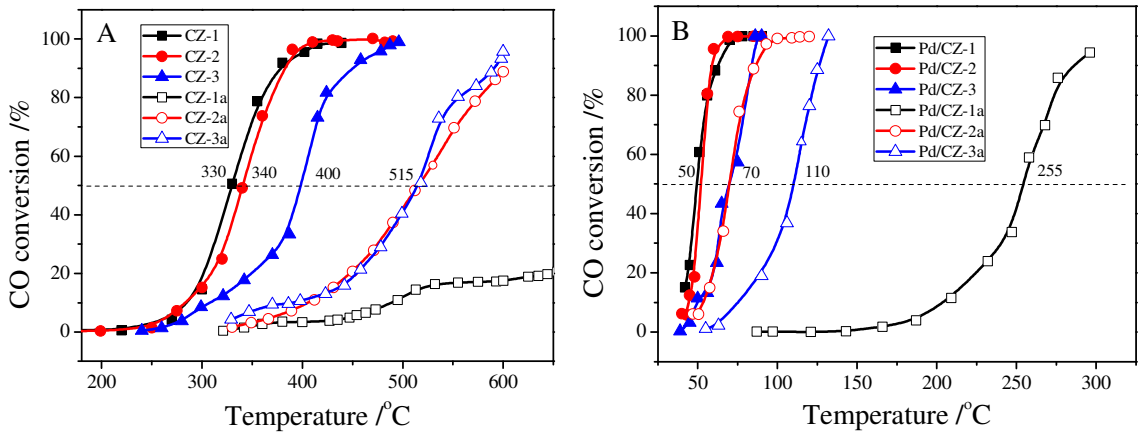

Fig. 11. Conversion of CO over (A) fresh and aged CZ, (B) fresh and aged 1wt.%Pd/CZ. (1000 ppm CO + 20% O_2+ 5%H_2O/Ar, GHSV of 30000 h^{-1})

4. Conclusions

In summary, a new method of the complexing-coprecipitation (CC) for the preparation of the Ce-Zr solid solution was designed, and by the help of this method more homogeneously nanodespersed and porous $Ce_{0.5}Zr_{0.5}O_2$ (CZ-2) particles was successfully prepared. Based on the characterizations of structural, textural and physicochemical properties of samples, it was found that $Ce_{0.5}Zr_{0.5}O_2$ prepared by the CC method existed as the *t*''-phase with rich oxygen defects and surface Ce^{3+}, and has bigger specific surface area, uniform particle and pore sizes, excellent bulk oxygen migration and redox abilities than the samples prepared by the co-precipitation method or complexing -coprecipitation-solution method. After this CZ-2 sample was calcined at 1100 °C for 6 h, its surface area, OSC (and OSCC, oxygen storage capacity complete) and catalytic activity for the oxidation of CO was still the best among three Ce-Zr solid solutions prepared by three methods whether it was used as the catalyst or support for Pd catalyst, reflecting its good

thermostability, though its particle and pore size was some increased. These results show that the physicochemical properties and catalytic activity for the CO oxidation as well as the redox behaviors (or OSC and OSCC) of the $Ce_{0.5}Zr_{0.5}O_2$ solid solutions strongly depend on the preparation methods. This complexing-coprecipitation (CC) method is a very effective and simple route to prepare the high oxygen storage capacity and thermal stable ceria-zirconia solid solutions.

Acknowledgements

This project was supported financially by the National Natural Science Foundation of China (21273150, 21171055), the National Basic Research Program of China (2013CB933201), the National High Technology Research and Development Program of China (2011AA03A406, 2012AA111717), and Fundamental Research Funds for the Central Universities (WK1214007).

References

1 B. Zhao, G.Li, C. Ge, Q. Wang and R. Zhou, *Appl. Catal. B*, 2010, **96**, 338-349.

2 Q. Liang, X. Wu, D. Weng and Z. Lu, *Catal. Commun*., 2008, **9**, 202-206.

3 L. Liu, Z. Yao, B. Liu and L. Dong, *J. Catal*., 2010, **275**, 45-60.

4 L. Liu, Y. Chen, L. Dong, J. Zhu, H. Wan, B. Liu, B. Zhao, H. Zhu, K. Sun, L. Dong and Y. Chen, *Appl. Catal. B*, 2009, **90**, 105-114.

5 M. Kantcheva, O. Samarkaya, L. Ilieva, G. Pantaleo, A.M. Venezia and D. Andreeva, *Appl. Catal. B*, 2009, **88**, 113-126.

6 P. Esteves, Y. Wu, C. Dujardin and P. Granger, *Catal. Today*, 2011, **176**, 453-457.

7 W. Cai, Q. Zhong and Y. Zhao, *Catal. Commun*., 2013, **39,** 30-34.

8 L. Zhang, D. Weng, B. Wang and X. Wu, *Catal. Commun*., 2010, **11**, 1229-1232.

9 D. Sellick, A. Aranda, T. García, J. López, B. Solsona, A. Mastral, D. Morgan, A. Carley and S. Taylor, *Appl. Catal. B*, 2013, **132-133**, 98-106.

10 Z. Wang, Z. Qu, X. Quan and H. Wang, *Appl. Catal. A*, 2012, **411-412**, 131-138.

11 C. Kalamaras, D. Dionysiou and A. Efstathiou, *ACS Catal*., 2012, **2**, 2729-2742.

12 W. Han, P. Zhang, Z. Tang, X. Pan and G. Lu, *J. Sol-Gel. Sci. Technol*., 2013, **66**, 526-532.

13 C. Hori, H. Permana, K. Simon Ng, A. Brenner, K. More, K. Rahmoeller and D. Belton, *Appl. Catal. B*, 1998, **16**, 105-117.

14 J. González-Velasco, M. Gutiérrez-Ortiz, J. Marc, J. Botas, M. González-Marcos and G. Blanchard, *Ind.*

Eng. Chem. Res., 2003, **42**, 311-317.

15 J. Fan, X. Wu, R. Ran and D. Weng, *Appl. Surf. Sci*., 2005, **245**, 162-171.

16 J. Anderson, R. Daley, S. Christou and A. Efstathiou, *Appl. Catal. B*, 2006, **64**, 189-200.

17 Y. Guo, G. Lu, Z. Zhang, S. Zhang, Y. Qi and Y. Liu, *Catal. Today*, 2007, **126**, 296-302.

18 Y. Nagai, T. Yamamoto, T. Nonaka, S. Yoshida, T. Nonaka, T. Okamoto, A. Suda and M. Sugiura, *Catal. Today*, 2002, **74**, 225-234.

19 A. Laachir, V. Perrichon, A. Badri, J. Lamotte, E. Catherine, J.C. Lavalley, J. El Fallah, L. Hilarie, F. Le Normand, E. Quemere, G.N. Sauvion and O. Touret, *J. Chem. Soc., Faraday Trans*., 1991, **87**, 1601-1609.

20 H.Y. Li, H.F. Wang, X.Q. Gong, Y.L. Guo, Y. Guo, G.Z. Lu and P. Hu, *Phys. Rev. B*, 2009, **79**, 193401-4.

21 S. Damyanova, B. Pawelec, K. Arishtirova, M.V. Martinez Huerta and J.L.G. Fierro, *Appl. Catal. A*, 2008, **337**, 86-96.

22 W.C. Zhan, Y. Guo, X.Q. Gong, Y.L. Guo, Y.Q. Wang and G.Z. Lu, *Chin. J. Catal*., 2014, **35**, 1238-1250.

23 H.F. Wang, X.Q. Gong, Y.L. Guo, Y. Guo, G.Z. Lu and P. Hu, *J. Phys. Chem. C,* 2009, **113**, 10229-10232.

24 W.C. Zhan, Y. Guo, Y.L. Guo, X.Q. Gong, Y.Q. Wang and G.Z. Lu, *SCIENTIA SINICA Chimica*, 2012, **42,** 1289-1307

25 S. Letichevsky, C. Tellez, R. De avillez, M. Da Silva, M. Fraga and L. Appel, *Appl. Catal. B*, 2005, **58**, 203-210.

26 E. Aneggi, C. De Leitenburg and A. Trovarelli, *Catal. Today*, 2012, **181**, 108-115.

27 Y. Liu, C. Wen, Y. Guo, G. Lu and Y. Wang, *J. Phys. Chem. C*, 2010, **114**, 9889-9897.

28 M. Thammachart, V. Meeyoo, T. Risksomboon and S. Osuwan, *Catal. Today*, 2001, **68**, 53-61.

29 A. Kozlov, D. Kim, A. Yezerets, P. Andersen, H. Kung and M. Kung, *J. Catal.*, 2002, **209**, 417-426.

30 M. Alifanti, B. Baps, N. Blangenois, J. Naud, P. Grange and B. Delmon, *Chem. Mater*., 2003, **15**, 395-403.

31 M. Epifani, T. Andreu, S. Abdollahzadeh-Ghom, J. Arbiol and J.R. Morante, *Adv. Funt. Mater.*, 2012, **22**, 2867-2875.

32 J. Kim, W. Myeong and S. Ihm, *J. Catal*., 2009, **263**, 123-133.

33 N. Laosiripojana and S. Assabumrungrat, *Appl. Catal. B*, 2005, **60**, 107-116.

34 X. Liang, X. Wang, Y. Zhuang, B. Xu, S. Kuang and Y. Li, *J. Am. Chem. Soc*., 2008, **130**, 2736-2737.

35 J. Wang, M. Shen, Y. An and J. Wang, *Catal. Commun*., 2008, **10**, 103-107.

36 Q.Y. Wang, G.F. Li, B. Zhao, M.Q. Shen and R.X. Zhou, *Appl. Catal. B*, 2010, **101**, 150-159.

37 G. Li, Q. Wang, B. Zhao and R. Zhou, *Appl. Catal. B*, 2011, **105**, 151-162.

38 Q. Wang, G. Li, B. Zhao and R. Zhou, *J. Hazar. Mater*., 2011, **189**, 150-157.

39 P. Huang, H. Jiang and M. Zhang, *J. Rare Earths*, 2012, **30**, 524-528.

40 Q. Wang, G. Li, B. Zhao and R. Zhou, *J. Mol. Catal. A*, 2011, **339**, 52-60.

41 V. Raju, S. Jaenicke and G. Chuah, *Appl. Catal. B*, 2009, **91**, 92-100.

42 R. Si, Y. Zhang, L. Wang, S. Li, B. Lin, W. Chu, Z. Wu and C. Yan, *J. Phys. Chem. C*, 2007, **111**, 787-794.

43 H.F. Wang, X.Q. Gong, Y.L. Guo, Y. Guo, G.Z. Lu and P. Hu, *Angew. Chem. Int. Ed*., 2009, **48**, 8289-8292.

44 G. Vlaic, P. Fornasiero, S. Geremia, J. Kašpar and M. Graziani, *J. Catal*., 1997, **168**, 386-392.

45 S. Lemaux, A. Bensaddik, A. Van der Eerden, J. Bitter and D. Koningsberger, *J. Phys. Chem. B*, 2001, **105**, 4810-4815.

46 M. Yashima, T. Sekikawa, D. Sato, H. Nakano and K. Omoto, *Cryst. Growth Des*., 2013, **13**, 829-837.

47 G. Li, B. Zhao, Q. Wang and R. Zhou, *Appl. Catal. B*, 2010, **97**, 41-48.

48 X. Weng, B. Perston, X. Wang, I. Arahams, T. Lin, S. Yang, J. Evans, D. Morgan, A. Carley, M. Bowker, J. Knowles, I. Rehman and J. Darr, *Appl. Catal. B*, 2009, **90**, 405-415.

49 M. Daturi, E. Finocchio, C. Binet, J.-C. Lavalley, F. Fally, V. Perrichon, H. Vidal, N. Hickey and J. Kašpar, *J. Phys. Chem. B*, 2000, **104**, 9186-9194.

50 R. Di Monte and J. Kašpar, *J. Mater. Chem*., 2005, **15**, 633-648.

51 P. Fornasiero, G. Balducci, R. Di Monte, J. Kašpar, V. Sergo, G. Gubitosa, A. Ferrero and M. Graziani, *J. Catal*., 1996, **164**, 173-183.

52 T. Murota, T. Hasegawa, S. Aozasa, H. Matsui and M. Motoyama, *J. Alloys Compd.*, 1993, **193**, 298-299.

53 L.H. Reddy, G.K. Reddy, D. Devaiah and B.M. Reddy, *Appl. Catal. A*, 2012, **445-446**, 297-305.

54 E. Mamontov, T, Eganmi, R. Brezny, M. Koranne and S. Tyagi, *J. Phys. Chem. B,* 2000, **104**, 11110-11116.

55 L. Liotta, A. Longo, A. Macaluso, A. Martorana, G. Pantaleo, A. Venzia and G. Deganello, *Appl. Catal. B*, 2004, **48**, 133-149.

56 J. Fan, X. Wu, X. Wu, Q. Liang, R. Ran and D. Weng, *Appl. Catal. B*, 2008, **81**, 38-48.

57 M. Alexandrou and R.M. Nix, *Surf. Sci*., 1994, **321**, 47-57.

58 Q. Wang, D. Li, B. Zhao and R. Zhou, *Appl. Catal. B*, 2010, **100**, 516-528.

59 X.H. Wang, G.Z. Lu, Y. Guo, L.Z. Jiang, Y.L. Guo and C.Z. Li, *J. Mater. Sci*., 2009, **44**, 1294-1301.

60 G.N. Li, L. Li, Y. Yuan, J.J. Shi, Y.Y. Yuan,Y.S. Li, W.R. Zhao, J.L. Shi, *Appl. Catal. B*, 2014, **158–159,** 341-347.

Graphic abstract:

Preparation and characterization of high oxygen storage capacity and thermally stable ceria-zirconia solid solution

Jie Li, Wangcheng Zhan, Yun Guo, Yanglong Guo, Guanzhong Lu*

* *Key Laboratory for Advanced Materials and Research Institute of Industrial Catalysis, East China University of Science and Technology, Shanghai, 200237, P. R. China.*

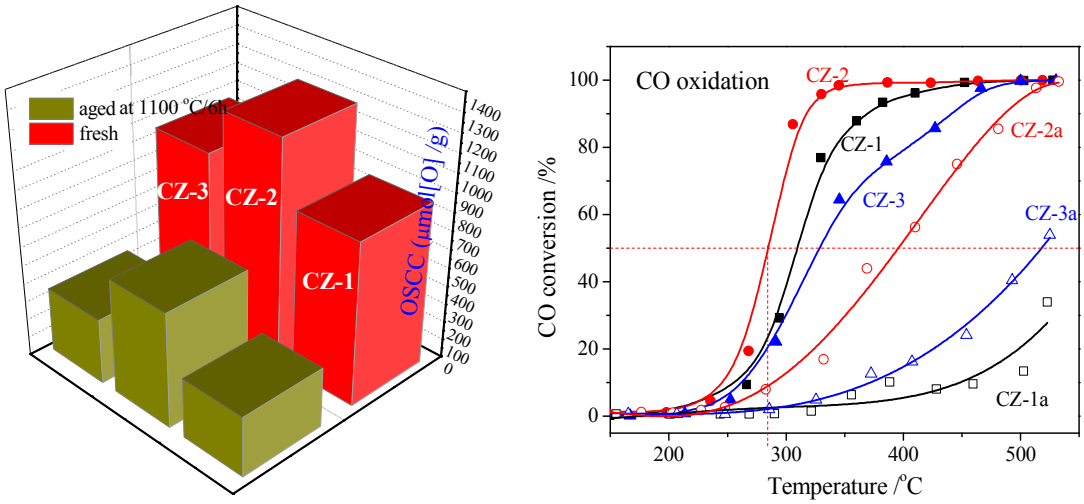

$Ce_{0.5}Zr_{0.5}O_2$ prepared by the complexing-coprecipitation method (CZ-2) exhibits the higher oxygen storage capacity (OSC) and thermal stability than the one prepared by Co-precipitation (CZ-1) or Complexing-coprecipitation-solution (CZ-3) method. After being aged at 1100 °C for 6 h, CZ-2a exhibited the highest OSC and catalytic activity.